Experimental Implementation of Universal Holonomic Quantum Computation on Solid-State Spins with Optimal Control

Yang Dong,[1,2] Shao-Chun Zhang,[1,2] Yu Zheng,[1,2] Hao-Bin Lin,[1,2] Long-Kun Shan,[1,2] Xiang-Dong Chen,[1,2] Wei Zhu,[3] Guan-Zhong Wang,[3] Guang-Can Guo,[1,2] and Fang-Wen Sun[1,2,*]

[1] *CAS Key Laboratory of Quantum Information, University of Science and Technology of China, Hefei 230026, People's Republic of China*

[2] *CAS Center for Excellence in Quantum Information and Quantum Physics, University of Science and Technology of China, Hefei 230026, People's Republic of China*

[3] *Hefei National Laboratory for Physical Science at Microscale, and Department of Physics, University of Science and Technology of China, Hefei, Anhui 230026, People's Republic of China*

(Received 8 September 2020; revised 9 June 2021; accepted 17 August 2021; published 31 August 2021)

Experimental realization of a universal set of quantum logic gates with high fidelity is critical to quantum-information processing, which is always challenging due to the inevitable interaction between the quantum system and environment. Geometric quantum computation is noise immune, and thus, offers a robust way to enhance control fidelity. Here, we experimentally implement the recently proposed extensible nonadiabatic holonomic quantum computation with solid spins in diamond at room temperature, which maintains both flexibility and resilience against decoherence and system-control errors. Compared with the previous geometric method, the fidelities of a universal set of holonomic single-qubit and two-qubit quantum logic gates are improved in experiments. Therefore, this work makes a step towards high-fidelity quantum-information processing based on extensible nonadiabatic holonomic quantum computation in realistic systems.

DOI: 10.1103/PhysRevApplied.16.024060

I. INTRODUCTION

Based on quantum superposition and entanglement [1–3], quantum-information processing can offer a dramatic increase in speed over classical methods in simulations [1,4], prime factoring [5], database searching [6], machine learning [7], and so on. Currently, as quantum coherence [2] is fragile under noise from either realistic environments or control fields, one of the most urgent requirements of quantum computation is to realize an error-resilient universal set of single-qubit and two-qubit gates [8–11]. By employing a composite pulse with dynamical control, gate fidelity can be enhanced systematically at the cost of a significant amount of operation time [12–14]. Compared with the dynamical control that depends on the instantaneous value of the Hamiltonian of a quantum system, geometric phases depend only on the global property of an enclosed path, and thus, have built-in noise-resilient features against certain local noise [15–20]. Moreover, if the quantum system has degenerate eigenstates, the geometric phase can act on the degenerate subspace [21,22] and is a key recipe for achieving high-fidelity quantum gates and constructing a full geometric quantum computation (GQC).

Originally, the GQC is constructed by adiabatic evolutions to avoid transitions between different energy-level states, and the logic gates depend only on the ratio of control parameters, which are immune to fluctuations in their absolute values [23,24]. However, the adiabatic condition simultaneously requires a long run time, and thus, decoherence will introduce considerable errors [25–28]. To overcome such an intrinsic disadvantage, nonadiabatic holonomic quantum computation (NHQC) schemes are proposed in theory based on a driving-system Hamiltonian with time-independent eigenstates [15,29]. Compared with the adiabatic case, this scheme is fast and is experimentally demonstrated in superconducting circuits [25,30], nuclear magnetic resonance [31,32], solid-spin systems [18,33–35], and trapped ions [36]. However, because of the challenges of exquisite control among quantum systems, systematic errors will introduce additional fluctuating phase shifts and lead to a serious reduction of fidelity compared with dynamical gates [23,37,38]. To make quantum operation robust against control errors and decoherence, the combination of NHQC and decoherence-mitigation methods, such as dynamical decoupling, decoherence-free subspaces [29], and quantum-error correction [39], is a promising strategy [40]. Recently, an extensible version of the NHQC+ scheme [41,42], which is robust against control errors without decoherence-mitigation methods by

*fwsun@ustc.edu.cn

relieving the parametric constraints of the original case, was proposed. In the experiment, only single-qubit operation was demonstrated in a superconducting circuit [25] and trapped ions [43]. It is still a nontrivial task to realize two-qubit gates based on the NHQC+ scheme due to the challenging requirement for exquisite control over complicated energy-level structures in experiments [25,26,43].

Here, based on the NHQC+ scheme [41,42], we experimentally demonstrate high-fidelity single-qubit and two-qubit holonomic quantum gates, which together make a universal gate set, all by nonadiabatically manipulating spin states in a diamond nitrogen-vacancy (N-V) center using a significantly simplified single-loop evolution. By shaping both amplitudes and phases of two microwave fields, we show explicitly in experiments that the NHQC+ scheme is robust against significant variations in control parameters. As a typical hybrid solid-spin system, the N-V center's electronic spin ($S = 1$) coupled with a nitrogen nuclear spin ($I = 1$) shows several intrinsic properties for the NHQC+ scheme. It also poses some challenges in experiments, mostly because the characteristic properties of the two types of spins differ by 3 orders of magnitude. The electron-spin dephasing time is usually shorter than typical durations of gates applied to nitrogen spin. Here, we apply a dynamical decoupling method [41,44] in the scheme to achieve high-fidelity nontrivial nonadiabatic holonomic two-qubit gates in experiments. Therefore, based on the NHQC+ scheme, a programmable solid-state quantum-information processor can be constructed efficiently at room temperature. Moreover, the geometric phase has a close relationship with the topological phase. The demonstration of robust holonomic quantum gates is a critical step towards the realization of topological quantum computation [45,46].

II. NHQC+ SCHEME WITH N-V CENTER

First, we explain how to implement the holonomic single-qubit gates in experiments. We manipulate the electron-spin states of the N-V center in synthetic diamond [47,49] at room temperature, as shown in Fig. 1(a). We encode $|m_s = -1\rangle \equiv |0\rangle$ and $|m_s = 1\rangle \equiv |1\rangle$ as the qubit basis states and use $|m_s = 0\rangle \equiv |a\rangle$ as an ancillary state for geometric manipulation, as shown in Fig. 1(b). The electron-spin state is initialized to $|m_s = 0\rangle$ by optical pumping and read out by identifying the distinct fluorescence intensity of the states after a 300-ns green-laser pulse. We apply a magnetic field of 378 G along the N-V axis using a permanent magnet. Under this magnetic field, the nearby nuclear spin can be optically polarized through level anticrossing, enhancing the coherence time of the electron spin [3] with $T_2^* \approx 8\ \mu$s and $T_2 \approx 600\ \mu$s, which are obtained from Ramsey and spin-echo signals, respectively.

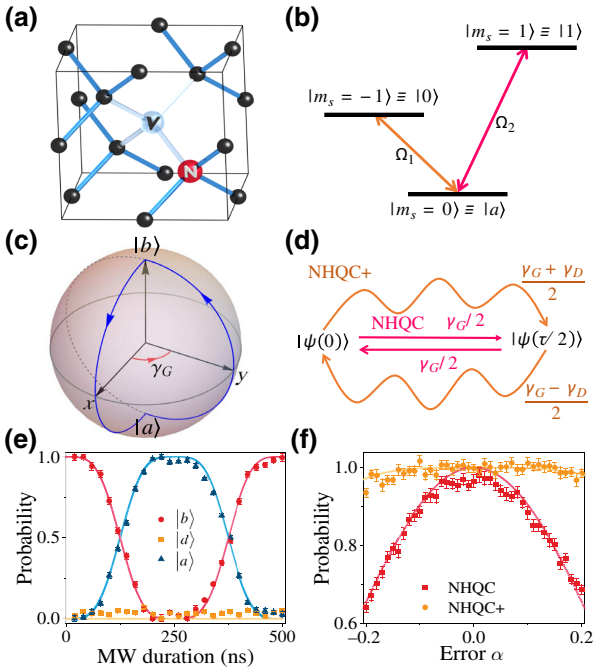

FIG. 1. (a) Schematic of the unit cell of diamond, including an N-V center. (b) Encoding of a qubit in the spin-triplet ground state and microwave coupling configuration. (c) Conceptual explanation of geometric quantum operation in the Bloch sphere, showing the geometric phase that equals half of the enclosed solid angle, γ_G. (d) Schematic of different paths for the NHQC (red) and NHQC+ (brown) with optimization methods. (e) Holonomic X gate on a bright state. Experimental results (dots) fit well with simulations (solid lines) with $\eta = 1$. (f) Performance of an X gate with control errors (α) for NHQC and NHQC+ schemes with initial state $|0\rangle$. Envelopes of the two driving fields of NHQC are truncated Gaussian pulses [18,19].

We apply microwave (MW) pulses to couple the transition from the ancillary level $|a\rangle$ to the qubit states $|0\rangle$ and $|1\rangle$ with Rabi frequencies $\Omega_1(t)$ and $\Omega_2(t)$, respectively, as shown in Fig. 1(b). The Hamiltonian for the couplings between these three levels takes the form

$$H_1 = \left[\frac{\Omega_1(t)}{2}e^{-i\phi_1}|0\rangle + \frac{\Omega_2(t)}{2}e^{-i\phi_2}|1\rangle\right]\langle a| + \text{H.c.}$$
$$= \frac{\Omega}{2}e^{-i\phi_1}|b\rangle\langle a| + \text{H.c.}, \quad (1)$$

where $\Omega = \sqrt{\Omega_1^2 + \Omega_2^2}$, and the bright state is $|b\rangle = \sin(\theta/2)|0\rangle - \cos(\theta/2)e^{i\phi}|1\rangle$ with $\tan(\theta/2) = \Omega_1/\Omega_2$ and $\phi = \phi_1 - \phi_2 - \pi$. In the NHQC+ scheme, θ and ϕ are time independent. Correspondingly, the dark state, $|d\rangle = \cos(\theta/2)|0\rangle + \sin(\theta/2)e^{i\phi}|1\rangle$, is decoupled from the $\{|b\rangle, |a\rangle\}$ subspace. Here, we choose the dark state and an orthogonal state, $|\psi\rangle = e^{-if/2}[\cos(\beta/2)e^{-i\varphi/2}|b\rangle + \sin(\beta/2)e^{i\varphi/2}|a\rangle]$, to demonstrate how to build up holonomic single-qubit gates. In the NHQC+ scheme, any

complete set of basis vectors satisfies the following conditions: (i) the cyclic evolution paths, $\Pi_1(0) = \Pi_1(\tau) = |d\rangle\langle d|$ and $\Pi_2(0) = \Pi_2(\tau) = |b\rangle\langle b|$; and (ii) the von Neumann equation, $(d/dt)\Pi_k(t) = -i[H_1, \Pi_k]$, where $\Pi_1(t) = |d\rangle\langle d|$ and $\Pi_2(t) = |\psi\rangle\langle\psi|$ denote the projectors. Using the von Neumann equation, we obtain the following coupled differential equations [42,43]: $\dot{f} = \dot{\varphi}/\cos\beta$, $\dot{\beta} = \Omega\sin(\varphi + \phi_1)$, and $\dot{\varphi} = \Omega\cot\beta\cos(\varphi + \phi_1)$, where the dot represents the time differential.

As shown in Fig. 1(c), we adopt a single-loop evolution path to induce a pure geometric phase. Specifically, during the whole cyclic evolution time of τ, we set $\beta = \pi\sin^2(\pi t/\tau)$ and $f = \eta[2\beta - \sin(2\beta)]$. Here, the parameter η is the degree of error suppression [42]. When $\eta \to 0$, the current protocol implementation reduces to the previous NHQC case [42]. During the first time interval, $[0, \tau/2)$, we set $\varphi(t = 0) = 0$. For the following part, $t \in [\tau/2, \tau]$, we set $\varphi(t = \tau/2) = \gamma_G$ and $\varphi(\tau) = \gamma_G$ with a constant angle γ_G. Moreover, we invert the dynamical phase of the latter interval to be opposite to the former one, and thus, no dynamical phase will be accumulated finally. It is quite different from the original NHQC scheme, as shown Fig. 1(d), where the dynamical phase at each moment is zero due to stringent requirements [15,18,19]. As a result, the corresponding evolution operator based on the NHQC+ scheme takes the form $U(0,\tau) = |d\rangle\langle d| + e^{i\gamma_G}|b\rangle\langle b|$ in the $\{|d\rangle, |b\rangle\}$ subspace, which is a holonomic single-qubit gate in the computation basis $\{|0\rangle, |1\rangle\}$:

$$U(\theta,\phi,\gamma) = e^{i(\gamma_G/2)}e^{-i(\gamma_G/2)\mathbf{n}\cdot\sigma}. \tag{2}$$

It describes a rotation operation around the axis $\mathbf{n} = (\sin\theta\cos\phi, \sin\theta\sin\phi, \cos\theta)$ by an angle γ_G, with a global phase factor $\exp(i\gamma_G/2)$.

In experiments, we first observe the behavior of the states driven by H_1 with the same experimental setup as that outlined in Refs. [47,48]. We initialize the qubit to the bright state, $|b\rangle = |0\rangle - |1\rangle/\sqrt{2}$, and set $\theta = \pi/2$, $\phi = 0$, and $\gamma_G = \pi$ to construct an X gate. Then the bright state evolves under the X gate and is projected to $|a\rangle$, $|b\rangle$ and the dark state, $|d\rangle = |0\rangle + |1\rangle/\sqrt{2}$. The experimental results are shown in Fig. 1(e). At the end of the pulse sequence, the bright state will acquire a pure geometric phase. Also, the bright state is always decoupled from the dark state by $H_1|d\rangle = 0$. Furthermore, to show the robustness of the NHQC+ scheme, we perform an X-gate operation, flipping $|0\rangle$ to $|1\rangle$ with an error in the amplitude of the control pulse, where the maximum Rabi frequency, $\Omega_{\max}$, has some variation: $\Omega_{\max} = (1 + \alpha)\Omega$. The theoretical and experimental results are shown in Fig. 1(f). The probability of the final state in $|1\rangle$ is plotted as a function of α. The systematic errors of the original NHQC scheme lead to a serious reduction in gate fidelity, compared with dynamical gate and infidelity scales, of $\varepsilon \sim \alpha^2$, which agrees with numerical results [23,38]. However, for the NHQC+ scheme, fluctuation of the control field is suppressed with optimal control, and the gate infidelity is scaled by $\varepsilon \sim \alpha^4$, which is more robust than the previous scheme for a broad range of pulse errors [26,42,43].

III. SINGLE-QUBIT GATE

Then, we demonstrate implementation of the single-qubit holonomic gates in a single-loop path with the N-V center based on a similar procedure to that discussed above with $\eta = 0.4$. We characterize the holonomic single-qubit gate through a standard quantum-process-tomography (QPT) method [43,47], with experimental sequences shown in Fig. 2(a). The experimental process matrices, $\chi_{\text{expt.}}$, of four specific geometric gates, I, $X/2$, $Y/2$, and X, are shown in Fig. 2(b), with fidelities of 0.983(4), 0.975(5), 0.978(5), and 0.977(5), respectively. Here, the process fidelity is calculated through $F = \left|\text{Tr}\left(\chi_{\text{expt.}}\chi_{\text{id}}^{\dagger}\right)\right|$ by comparing it with the ideal operation, χ_{id}. The gate fidelities are better than those previously reported [18]. As the original QPT is implemented by dynamical operation [34] with a long run time, it is more prone to noise, parameter imperfection, and decoherence effects than a holonomic gate. However, for the NHQC+ scheme in our experiment, the gate time is much smaller than the coherence time of the N-V center [13]. Here, we can implement $X/2$ and $Y/2$ gates successively and perform QPT when the gates are repeated, as shown in Fig. 3. The average fidelity [13,18,50], N, of the NHQC+ gates can be calculated as follows: $F_N = \frac{1}{2} + \frac{1}{2}(1 - 2p)^N =$

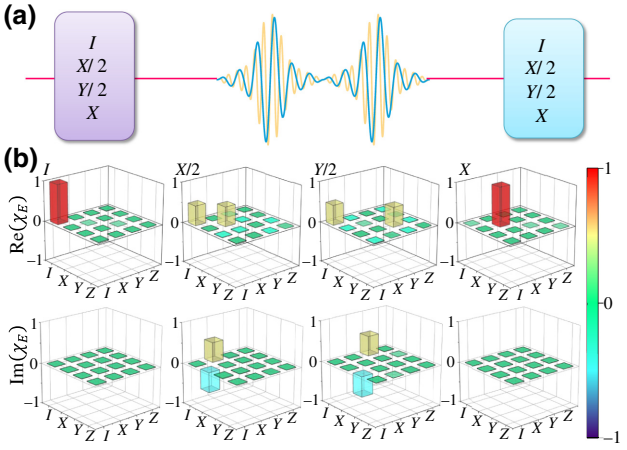

FIG. 2. QPT results of single-qubit operation. (a) Experimental pulse sequence to characterize the performance of the single-qubit gate. (b) Bar charts of the real and imaginary parts of χ_{exp} for specific gates I, $X/2$, $Y/2$, and X, giving fidelities of 0.983(4), 0.975(5), 0.978(5), and 0.977(5), respectively. Labels on the X and Y axes correspond to operators in the basis set $\{I, \sigma_x, \sigma_y, \sigma_z\}$ of the $\{|0\rangle, |1\rangle\}$ subspace. $X/2$ ($Y/2$) is a $\pi/2$ rotation around the x (y) axis in the Bloch sphere.

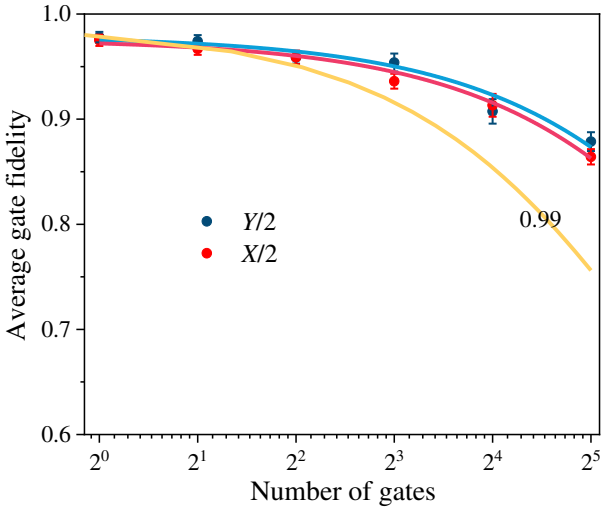

FIG. 3. Decay of the fidelity of nonadiabatic holonomic $X/2$ and $Y/2$ gates obtained via QPT. Experimental data for $X/2$ (red dots) and $Y/2$ (blue dots) gates are fitted by $F = \left[1 + (1 - \varepsilon_{\mathrm{IF}})\,(1 - 2p)^N\right]/2$ (solid line), and $\varepsilon_{\mathrm{IF}}$ describes errors in state preparation and measurement. Gold line represents the necessary fidelity threshold of 99% for the implementation of state-of-the-art error-correction codes based on surface codes.

$\frac{1}{2} + \frac{1}{2}\exp\left(-T/T_{1\rho}\right)$, where $T = N\tau$ and p is the average error per gate. We can estimate the average fidelity of $X/2$ and $Y/2$ gates to be $F_{X/2} = 1 - p_{X/2} = 0.9957(5)$ and $F_{Y/2} = 0.9961(4)$, respectively, from experimental data; these values exceed the threshold of necessary fidelity for the implementation of state-of-art error-correction codes based on surface codes [20]. By lowering the temperature [51], $T_{1,\rho}$ and T_2 can be prolonged by $3 - 6$ orders of magnitude in proportion to T_1, which means that the performance of the NHQC+ scheme can be improved significantly for solid quantum-information processing.

IV. TWO-QUBIT GATE

To realize a universal quantum computation, a two-qubit gate is also necessary. Here, we use the nonzero host-nitrogen nuclear spin ($I = 1$ for ^{14}N) of the N-V center as the target qubit, as shown in Fig. 4(a). The Hamiltonian can be expressed as

$$H_s = DS_z^2 + \gamma_e B S_z + P I_z^2 + \gamma_n B I_z + A_{zz} S_z I_z. \quad (3)$$

Here, S_z and I_z are the z components of the spin -1 operators for the electron and ^{14}N nuclear spins, respectively. γ_e and γ_N are the electronic and ^{14}N nuclear gyromagnetic ratios. The zero-field splitting is $D = 2.87$ GHz, the nuclear quadrupolar splitting is $P = -4.95$ MHz, and the hyperfine interaction between the N-V electron and the ^{14}N nuclear spin is $A = 2.16$ MHz. By applying state-selective MW and radio-frequency (rf) pulses, we can couple different energy levels. For arbitrary sublevels of the electron-spin ground state, the ^{14}N nuclear spin has a lambda (Λ) energy structure, which is preferable to realize the NHQC+ scheme [41,42]. Similarly, we encode $|m_I = -1\rangle \equiv |0\rangle$ and $|m_I = 1\rangle \equiv |1\rangle$ as the qubit basis states and use $|m_I = 0\rangle \equiv |a\rangle$ as an ancillary state for the geometric manipulation of the ^{14}N nuclear spin.

For a two-qubit gate, the target qubit is changed, depending on the state of the control qubit. The unitary operation for a controlled rotation (CROT) gate is equivalent to a controlled NOT (CNOT) gate [10,52]. A typical CROT gate can be represented as

$$U_{\mathrm{CROT}} = \begin{pmatrix} R_y(\pi) & 0 \\ 0 & 1 \end{pmatrix},$$

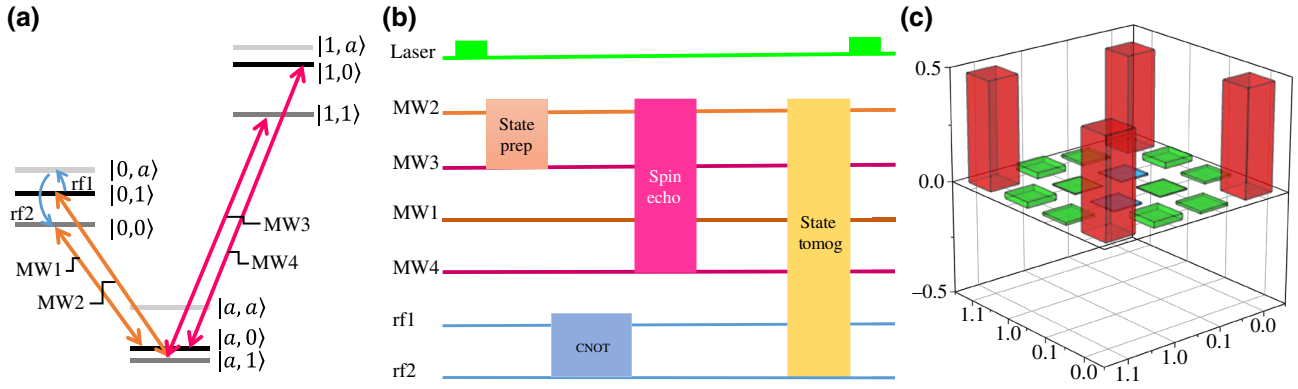

FIG. 4. (a) Level structures of electron and nuclear spins for the geometric CROT gate and the MW and rf coupling configuration. (b) Time sequence for the implementation and verification of the geometric CROT gate between electron and nuclear spins. CROT gate is implemented by applying rf1 and rf2 pulses simultaneously. Duration time for CROT gate is 42 μs. MW pulses are used to implement a spin echo to increase the N-V center's coherence time, and the selective MW sequence is $\pi_{\mathrm{MW3}} - \pi_{\mathrm{MW2}} - \pi_{\mathrm{MW1}} - \pi_{\mathrm{MW4}}$. To verify the CROT gate, we use a combination of MW1–MW4 and a rf to implement QST. (c) Matrix elements of the output density operator reconstructed through QST, where geometric CROT is applied to the product state $|0\rangle - |1\rangle/\sqrt{2}\,|1\rangle$.

TABLE I. Measured fidelities of the output states of the NHQC+ CROT gate with six typical input states.

Initial state	$\|11\rangle$	$\|01\rangle$	$(\|01\rangle - \|11\rangle)/\sqrt{2}$	$\|10\rangle$	$\|00\rangle$	$(\|00\rangle - \|10\rangle)/\sqrt{2}$
Final ideal state	$\|11\rangle$	$-\|00\rangle$	$-(\|00\rangle + \|11\rangle)/\sqrt{2}$	$\|10\rangle$	$\|01\rangle$	$(\|01\rangle - \|10\rangle)/\sqrt{2}$
Fidelity	0.973(8)	0.974(9)	0.952(5)	0.96(1)	0.962(9)	0.940(7)

where 1, 0, and $R_y(\pi)$ represent 2×2 matrices, corresponding to the unit operator, zero matrix, and a rotation matrix around the y axis with $R_y(\pi) = e^{-i\pi\sigma_y/2}$. Figure 4(b) shows the circuit model of the CROT gate. First, we initialize the hybrid quantum system to the auxiliary state, $|a, 1\rangle$, by the green laser. Then, by employing MW operation, the bright state of the electron spin, $|b, 1\rangle$, is prepared. Due to the magnetic dipole interaction, $A_{zz}S_zI_z$, the energy-level splitting of the ^{14}N nuclear spin depends on the electron-spin state. Assisting with state-selective rf pulses, we can apply a holonomic Y gate to the ^{14}N nuclear spin, which depends on the electron-spin state, as shown in Fig. 4(a). Hence, for such a solid hybrid-spin system, the two-qubit CROT gate can be implemented similarly to the single-qubit case. However, the duration of one CROT gate is long, so the decoherence effect destroys a significant part of the quantum information. To correct that, we apply a dynamical decoupling method to the scheme with spin-echo pulses [9,10,18,23] at the middle of the whole circuit, with the time sequence shown in Fig. 4(b). As an example, with an initial state of $|0\rangle - |1\rangle/\sqrt{2}\,|1\rangle$, the final state is detected by quantum-state tomography (QST). The experimental results are shown in Fig. 4(c). Compared with the ideal final state, $|00\rangle + |11\rangle/\sqrt{2}$, the measured entanglement fidelity is 95.2(5)%, which unambiguously confirms the entanglement and is higher than that obtained with previous protocols for the same system [18,23]. Furthermore, the measured final-state fidelities are listed in Table I for six typical input states for the holonomic two-qubit CROT gate.

V. CONCLUSION

We experimentally demonstrate a universal set of robust holonomic gates using individual spins, which paves the way for all-geometric quantum computation with a solid-state system. The noise-resilient feature of the realized single-qubit geometric gates is also verified by comparing the performances of NHQC and NHQC+ schemes. The distinct advantages of the realized NHQC+ scheme indicate that it is a promising candidate for robust quantum-information processing. Moreover, a nontrivial high-fidelity two-qubit CROT gate is preformed with this geometric protocol and enhanced by the dynamical decoupling method. Since the electron and nuclear spins of different N-V centers can be wired up quantum mechanically and magnetically by direct dipole interactions [53, 54], phonon-induced spin-spin interactions [55,56], and carbon-nanotube-mediated coupling [57,58], a scalable fault-tolerant quantum network is promising. Moreover, the NHQC+ protocols used here for the pure geometric implementation of universal gates should also be of interest to other physical systems, such as superconducting circuits, trapped ions, quantum dots, and nuclear magnetic resonance.

ACKNOWLEDGMENTS

We thank Bao-Jie Liu and Man-Hong Yung for valuable discussions. This work is supported by the National Key Research and Development Program of China (Grant No. 2017YFA0304504), the Science Challenge Project (Grant No. TZ2018003), the National Natural Science Foundation of China (Grants No. 91536219, No. 61522508, No. 91850102, and No. 12005218), the Anhui Initiative in Quantum Information Technologies (Grant No. AHY130000), and the Fundamental Research Funds for the Central Universities (Grant No. WK2030000020).

APPENDIX A: OPTIMAL CONTROL SEQUENCE

For the resonance NHQC+ scheme [42,43], two time-dependent parameters need to be controlled precisely, to enhance the robustness of quantum gates against control-amplitude fluctuation. Suppose there is an error (α) in control amplitude, the Hamiltonian of the system can be expressed as

$$H_1 = (1+\alpha)\frac{\Omega(t)}{2}e^{-i\phi_1(t)}|b\rangle\langle a| + \text{H.c.}. \tag{A1}$$

In our experiments, the influence of control-amplitude errors can be evaluated at the end of the first interval, $\tau/2$, and the probability amplitude error is given as

$$P = |\langle\psi(\tau/2) \mid \psi_\alpha(\tau/2)\rangle|^2 = 1 + O_1 + O_2 + \cdots, \tag{A2}$$

where $|\psi_\alpha\rangle$ is the state with the systematic control error, and O_m is the mth-order perturbation term. Here, we calculate only the probability amplitude to the second order as

$$P \simeq 1 - \alpha^2 \left| \int_0^{T/2} e^{-if}\,\dot{\beta}\sin^2\beta dt \right|^2. \tag{A3}$$

To nullify the error effect [42,43], we set $f = \eta[2\beta - \sin(2\beta)]$, $\varphi(t=0) = 0$, and $\varphi_2(t=\tau/2) = \gamma_G$, which lead

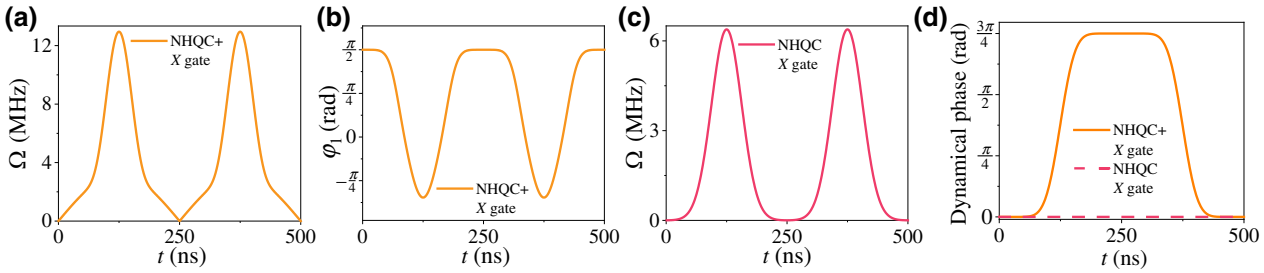

FIG. 5. (a),(b) Amplitude and phase of MW field used in experiments for the NHQC+ X gate. (c) Waveform pulse of 4σ-truncated Gaussian shape in the conventional NHQC X gate without phase modulation. (d) Dynamical phases of the X gate in NHQC+ (orange curve) and NHQC (red dashed line) schemes as a function of time t during the full evolution.

to $P = 1 - \alpha^2 \sin^2 \eta\pi/(2\eta)^2$. In the experimental demonstration, we select $\eta = 1$ to show the MW-control-field error resilience of the NHQC+ scheme [Fig. 5(a)], and the waveform is shown in Fig. 5(b). The typical 4σ-truncated Gaussian waveform of the MW for the NHQC protocol is shown in Fig. 5(c). The X gate can be realized in a single-loop way by keeping the relative MW phase unchanged [19].

APPENDIX B: DYNAMICAL PHASE IN NHQC+

In the construction of the NHQC+ gate, the dynamical phase can be cancelled out. As shown in Fig. 1(c), cyclic evolution with time τ is divided into two parts. During the first interval, $t \in [0, \tau/2)$, the initial value of $\varphi(t)$ is set to $\varphi(t = 0) = 0$, and $\varphi(\tau/2) = \int_0^{\tau/2} \dot{f} \cos\beta dt = 0$, where $\dot{f} = \dot{\varphi}/\cos\beta$, $\dot{\beta} = \Omega \sin(\varphi + \phi_1)$, and $\dot{\varphi} = \Omega \cot\beta \cos(\varphi + \phi_1)$. The corresponding evolution operator is $U_1(0, \tau/2) = |d\rangle\langle d| + e^{i\gamma_1}|a\rangle\langle b|$, where $\gamma_1 = -f(\tau/2)/2$. During the second interval, $t \in [\tau/2, \tau]$, we set $\varphi(t = \tau/2) = \gamma_G$ and $\varphi(t = \tau) = \int_{\tau/2}^{\tau} \dot{f} \cos\beta dt = \gamma_G$, with γ_G being an arbitrary constant angle. Then, the evolution operator is $U_2(\tau/2, \tau) = |d\rangle\langle d| + e^{i\gamma_2}|b\rangle\langle a|$, where $\gamma_2 = \gamma_G + f(\tau/2)/2$. In this way, the dynamical phase is cancelled out and the holonomic matrix is given by $U(0, \tau) = |d\rangle\langle d| + e^{i\gamma_G}|b\rangle\langle b|$. In comparison, there is a strict constraint imposed on the driving Hamiltonian for the NHQC scheme, to make the dynamical phase vanish during gate operations. Meanwhile, we plot the dynamical phases in NHQC+ and NHQC schemes during a whole X gate evolution, as shown in Fig. 5(d).

APPENDIX C: THE EFFECT OF η

The parameter η is the degree of error suppression. It seems that the optimized pulse is bounded by $\Omega_{\max}$, and thus, the improvement of the gate performance can only be attributed to optimal control [42]. But, in the case of $\eta \geq 1$, under the restriction, the gate duration time τ will be too long, and decoherence will introduce unacceptable gate infidelity. Hence, we need to confirm the optimal value of η under the targets with both a short time τ and low systematic error sensitivity. In experiments, we find that the robustness of the holonomic quantum gates in our scheme is significantly improved with $\eta = 0.4$, and the control sequence is shown in Fig. 6(a)–6(c). When $\eta \to 0$, the current implementation reduces to the previous NHQC case, and the infidelity of the quantum gate scales as $\varepsilon \sim \alpha^2$.

Hence, the NHQC+ scheme shares the same advantages as those of NHQC over adiabatic GQC for speeding up the operation times of quantum gates. In terms of systematic control-field errors, the NHQC+ protocol can become

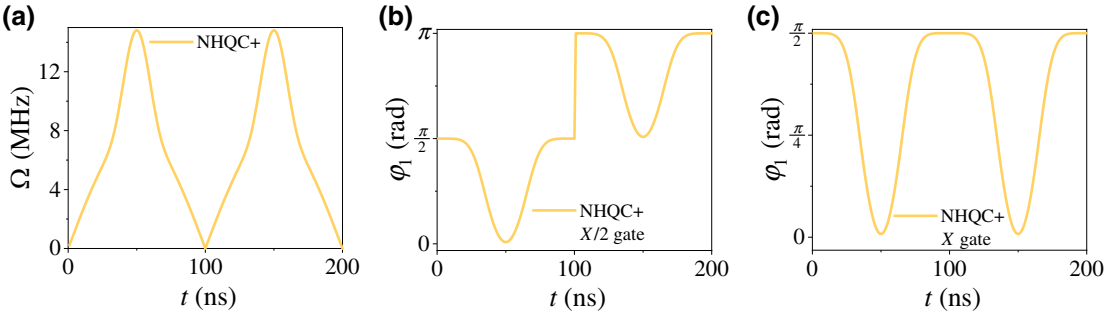

FIG. 6. (a) Amplitude of MW field in experiments for single-qubit holonomic gates. (b),(c) Phases of MW field used in experiments for NHQC+ $X/2$ and X gates with $\eta = 0.4$. For the $Y/2$ gate, $\phi = \pi/2$ and the amplitude- and phase-modulation sequence are the same as those of the $X/2$ gate.

potentially more robust. The reason is that this protocol removes the limitation of the pulse shape. Practically, the parameter paths are typically not unique and can be chosen from a family of solutions for experiments. To compare with the NHQC scheme, we keep the same gate duration in experiments, where a higher maximal MW power is needed for the NHQC+ scheme. Previous process fidelities based on the NHQC scheme [18] with the N-V center are $96.5\% \pm 1.9\%$, $96.9\% \pm 1.5\%$, and $92.1\% \pm 1.8\%$ for the NOT gate, the rotation gate, and the Hadamard gate, respectively; these values are lower than that with the NHQC+ scheme.

[1] T. Van der Sar, Z. Wang, M. Blok, H. Bernien, T. Taminiau, D. Toyli, D. Lidar, D. Awschalom, R. Hanson, and V. Dobrovitski, Decoherence-protected quantum gates for a hybrid solid-state spin register, Nature **484**, 82 (2012).

[2] A. Streltsov, G. Adesso, and M. B. Plenio, Colloquium: Quantum coherence as a resource, Rev. Mod. Phys. **89**, 041003 (2017).

[3] Y. Dong, Y. Zheng, S. Li, C.-C. Li, X.-D. Chen, G.-C. Guo, and F.-W. Sun, Non-markovianity-assisted high-fidelity deutsch–jozsa algorithm in diamond, npj Quantum Inf. **4**, 1 (2018).

[4] Y. Wu, W. Liu, J. Geng, X. Song, X. Ye, C.-K. Duan, X. Rong, and J. Du, Observation of parity-time symmetry breaking in a single-spin system, Science **364**, 878 (2019).

[5] X. Peng, Z. Liao, N. Xu, G. Qin, X. Zhou, D. Suter, and J. Du, Quantum Adiabatic Algorithm for Factorization and its Experimental Implementation, Phys. Rev. Lett. **101**, 220405 (2008).

[6] J. Zhang, S. S. Hegde, and D. Suter, Efficient Implementation of a Quantum Algorithm in a Single Nitrogen-Vacancy Center of Diamond, Phys. Rev. Lett. **125**, 030501 (2020).

[7] G. Carleo, I. Cirac, K. Cranmer, L. Daudet, M. Schuld, N. Tishby, L. Vogt-Maranto, and L. Zdeborová, Machine learning and the physical sciences, Rev. Mod. Phys. **91**, 045002 (2019).

[8] J. Casanova, Z.-Y. Wang, and M. B. Plenio, Noise-Resilient Quantum Computing with a Nitrogen-Vacancy Center and Nuclear Spins, Phys. Rev. Lett. **117**, 130502 (2016).

[9] J. Zhang, A. M. Souza, F. D. Brandao, and D. Suter, Protected Quantum Computing: Interleaving Gate Operations with Dynamical Decoupling Sequences, Phys. Rev. Lett. **112**, 050502 (2014).

[10] J. Zhang and D. Suter, Experimental Protection of Two-Qubit Quantum Gates against Environmental Noise by Dynamical Decoupling, Phys. Rev. Lett. **115**, 110502 (2015).

[11] D. A. Golter, T. K. Baldwin, and H. Wang, Protecting a Solid-State Spin from Decoherence Using Dressed Spin States, Phys. Rev. Lett. **113**, 237601 (2014).

[12] X. Wang, L. S. Bishop, E. Barnes, J. Kestner, and S. D. Sarma, Robust quantum gates for singlet-triplet spin qubits using composite pulses, Phys. Rev. A **89**, 022310 (2014).

[13] X. Rong, J. Geng, F. Shi, Y. Liu, K. Xu, W. Ma, F. Kong, Z. Jiang, Y. Wu, and J. Du, Experimental fault-tolerant universal quantum gates with solid-state spins under ambient conditions, Nat. Commun. **6**, 1 (2015).

[14] T. Nöbauer, A. Angerer, B. Bartels, M. Trupke, S. Rotter, J. Schmiedmayer, F. Mintert, and J. Majer, Smooth Optimal Quantum Control for Robust Solid-State Spin Magnetometry, Phys. Rev. Lett. **115**, 190801 (2015).

[15] E. Sjöqvist, D.-M. Tong, L. M. Andersson, B. Hessmo, M. Johansson, and K. Singh, Non-adiabatic holonomic quantum computation, New J. Phys. **14**, 103035 (2012).

[16] G. Xu, P. Zhao, D. Tong, and E. Sjöqvist, Robust paths to realize nonadiabatic holonomic gates, Phys. Rev. A **95**, 052349 (2017).

[17] N. Ramberg and E. Sjöqvist, Environment-Assisted Holonomic Quantum Maps, Phys. Rev. Lett. **122**, 140501 (2019).

[18] C. Zu, W.-B. Wang, L. He, W.-G. Zhang, C.-Y. Dai, F. Wang, and L.-M. Duan, Experimental realization of universal geometric quantum gates with solid-state spins, Nature **514**, 72 (2014).

[19] Y. Xu, W. Cai, Y. Ma, X. Mu, L. Hu, T. Chen, H. Wang, Y. Song, Z.-Y. Xue, and Z.-q. Yin, *et al.*, Single-Loop Realization of Arbitrary Nonadiabatic Holonomic Single-Qubit Quantum Gates in a Superconducting Circuit, Phys. Rev. Lett. **121**, 110501 (2018).

[20] F. Kleißler, A. Lazariev, and S. Arroyo-Camejo, Universal, high-fidelity quantum gates based on superadiabatic, geometric phases on a solid-state spin-qubit at room temperature, npj Quantum Inf. **4**, 1 (2018).

[21] L.-M. Duan, J. I. Cirac, and P. Zoller, Geometric manipulation of trapped ions for quantum computation, Science **292**, 1695 (2001).

[22] B.-J. Liu, Z.-H. Huang, Z.-Y. Xue, and X.-D. Zhang, Superadiabatic holonomic quantum computation in cavity qed, Phys. Rev. A **95**, 062308 (2017).

[23] Y.-Y. Huang, Y.-K. Wu, F. Wang, P.-Y. Hou, W.-B. Wang, W.-G. Zhang, W.-Q. Lian, Y.-Q. Liu, H.-Y. Wang, and H.-Y. Zhang, *et al.*, Experimental Realization of Robust Geometric Quantum Gates with Solid-State Spins, Phys. Rev. Lett. **122**, 010503 (2019).

[24] D. Guéry-Odelin, A. Ruschhaupt, A. Kiely, E. Torrontegui, S. Martínez-Garaot, and J. G. Muga, Shortcuts to adiabaticity: Concepts, methods, and applications, Rev. Mod. Phys. **91**, 045001 (2019).

[25] T. Yan, B.-J. Liu, K. Xu, C. Song, S. Liu, Z. Zhang, H. Deng, Z. Yan, H. Rong, and K. Huang, *et al.*, Experimental Realization of Nonadiabatic Shortcut to Non-Abelian Geometric Gates, Phys. Rev. Lett. **122**, 080501 (2019).

[26] Y. Xu, Z. Hua, T. Chen, X. Pan, X. Li, J. Han, W. Cai, Y. Ma, H. Wang, and Y. Song, *et al.*, Experimental Implementation of Universal Nonadiabatic Geometric Quantum Gates in a Superconducting Circuit, Phys. Rev. Lett. **124**, 230503 (2020).

[27] K. Zhang, N. Nusran, B. Slezak, and M. G. Dutt, Experimental limits on the fidelity of adiabatic geometric phase gates in a single solid-state spin qubit, New J. Phys. **18**, 053029 (2016).

[28] E. Boyers, M. Pandey, D. K. Campbell, A. Polkovnikov, D. Sels, and A. O. Sushkov, Floquet-engineered quantum state

manipulation in a noisy qubit, Phys. Rev. A **100**, 012341 (2019).
[29] G. Xu, J. Zhang, D. Tong, E. Sjöqvist, and L. Kwek, Nonadiabatic Holonomic Quantum Computation in Decoherence-Free Subspaces, Phys. Rev. Lett. **109**, 170501 (2012).
[30] A. A. Abdumalikov Jr, J. M. Fink, K. Juliusson, M. Pechal, S. Berger, A. Wallraff, and S. Filipp, Experimental realization of non-abelian non-adiabatic geometric gates, Nature **496**, 482 (2013).
[31] G. Feng, G. Xu, and G. Long, Experimental Realization of Nonadiabatic Holonomic Quantum Computation, Phys. Rev. Lett. **110**, 190501 (2013).
[32] Z. Zhu, T. Chen, X. Yang, J. Bian, Z.-Y. Xue, and X. Peng, Single-Loop and Composite-Loop Realization of Nonadiabatic Holonomic Quantum Gates in a Decoherence-Free Subspace, Phys. Rev. Appl. **12**, 024024 (2019).
[33] K. Nagata, K. Kuramitani, Y. Sekiguchi, and H. Kosaka, Universal holonomic quantum gates over geometric spin qubits with polarised microwaves, Nat. Commun. **9**, 1 (2018).
[34] S. Arroyo-Camejo, A. Lazariev, S. W. Hell, and G. Balasubramanian, Room temperature high-fidelity holonomic single-qubit gate on a solid-state spin, Nat. Commun. **5**, 4870 (2014).
[35] B. B. Zhou, P. C. Jerger, V. O. Shkolnikov, F. J. Heremans, G. Burkard, and D. D. Awschalom, Holonomic Quantum Control by Coherent Optical Excitation in Diamond, Phys. Rev. Lett. **119**, 140503 (2017).
[36] F. Leroux, K. Pandey, R. Rehbi, F. Chevy, C. Miniatura, B. Grémaud, and D. Wilkowski, Non-abelian adiabatic geometric transformations in a cold strontium gas, Nat. Commun. **9**, 1 (2018).
[37] M. Johansson, E. Sjöqvist, L. M. Andersson, M. Ericsson, B. Hessmo, K. Singh, and D. Tong, Robustness of nonadiabatic holonomic gates, Phys. Rev. A **86**, 062322 (2012).
[38] S.-B. Zheng, C.-P. Yang, and F. Nori, Comparison of the sensitivity to systematic errors between nonadiabatic non-abelian geometric gates and their dynamical counterparts, Phys. Rev. A **93**, 032313 (2016).
[39] C. Wu, Y. Wang, X.-L. Feng, and J.-L. Chen, Holonomic Quantum Computation in Surface Codes, Phys. Rev. Appl. **13**, 014055 (2020).
[40] P. Zhao, X. Wu, and D. Tong, Dynamical-decoupling-protected nonadiabatic holonomic quantum computation, Phys. Rev. A **103**, 012205 (2021).
[41] B.-J. Liu, X.-K. Song, Z.-Y. Xue, X. Wang, and M.-H. Yung, Plug-And-Play Approach to Nonadiabatic Geometric Quantum Gates, Phys. Rev. Lett. **123**, 100501 (2019).
[42] S. Li, T. Chen, and Z.-Y. Xue, Fast holonomic quantum computation on superconducting circuits with optimal control, Adv. Quantum Technol. **3**, 2000001 (2020).
[43] M.-Z. Ai, S. Li, Z. Hou, R. He, Z.-H. Qian, Z.-Y. Xue, J.-M. Cui, Y.-F. Huang, C.-F. Li, and G.-C. Guo, Experimental Realization of Nonadiabatic Holonomic Single-Qubit Quantum Gates with Optimal Control in a Trapped ion, Phys. Rev. Appl. **14**, 054062 (2020).
[44] Y. Dong, X.-D. Chen, G.-C. Guo, and F.-W. Sun, Reviving the precision of multiple entangled probes in an open system by simple π-pulse sequences, Phys. Rev. A **94**, 052322 (2016).
[45] C. Nayak, S. H. Simon, A. Stern, M. Freedman, and S. D. Sarma, Non-abelian anyons and topological quantum computation, Rev. Mod. Phys. **80**, 1083 (2008).
[46] B. Li, P.-B. Li, Y. Zhou, J. Liu, H.-R. Li, and F.-L. Li, *et al.*, Interfacing a Topological Qubit with a Spin Qubit in a Hybrid Quantum System, Phys. Rev. Appl. **11**, 044026 (2019).
[47] Y. Dong, S.-C. Zhang, H.-B. Lin, X.-D. Chen, W. Zhu, G.-Z. Wang, G.-C. Guo, and F.-W. Sun, Quantifying the performance of multipulse quantum sensing, Phys. Rev. B **103**, 104104 (2021).
[48] Y. Dong, J.-Y. Xu, S.-C. Zhang, Y. Zheng, X.-D. Chen, W. Zhu, G.-Z. Wang, G.-C. Guo, and F.-W. Sun, Composite-pulse enhanced room-temperature diamond magnetometry, Funct. Diamond **1**, 125 (2021).
[49] C.-H. Li, Y. Dong, J.-Y. Xu, D.-F. Li, X.-D. Chen, A. Du, Y.-S. Ge, G.-C. Guo, and F.-W. Sun, Enhancing the sensitivity of a single electron spin sensor by multi-frequency control, Appl. Phys. Lett. **113**, 072401 (2018).
[50] X. Rong, J. Geng, Z. Wang, Q. Zhang, C. Ju, F. Shi, C.-K. Duan, and J. Du, Implementation of Dynamically Corrected Gates on a Single Electron Spin in Diamond, Phys. Rev. Lett. **112**, 050503 (2014).
[51] T. Astner, J. Gugler, A. Angerer, S. Wald, S. Putz, N. J. Mauser, M. Trupke, H. Sumiya, S. Onoda, and J. Isoya, *et al.*, Solid-state electron spin lifetime limited by phononic vacuum modes, Nat. Mater. **17**, 313 (2018).
[52] F. Jelezko, T. Gaebel, I. Popa, M. Domhan, A. Gruber, and J. Wrachtrup, Observation of Coherent Oscillation of a Single Nuclear Spin and Realization of a Two-Qubit Conditional Quantum Gate, Phys. Rev. Lett. **93**, 130501 (2004).
[53] F. Dolde, I. Jakobi, B. Naydenov, N. Zhao, S. Pezzagna, C. Trautmann, J. Meijer, P. Neumann, F. Jelezko, and J. Wrachtrup, Room-temperature entanglement between single defect spins in diamond, Nat. Phys. **9**, 139 (2013).
[54] C. Bradley, J. Randall, M. Abobeih, R. Berrevoets, M. Degen, M. Bakker, M. Markham, D. Twitchen, and T. Taminiau, A Ten-Qubit Solid-State Spin Register with Quantum Memory up to one Minute, Phys. Rev. X **9**, 031045 (2019).
[55] M. C. Kuzyk and H. Wang, Scaling Phononic Quantum Networks of Solid-State Spins with Closed Mechanical Subsystems, Phys. Rev. X **8**, 041027 (2018).
[56] D. Maroulakos, L. Chotorlishvili, D. Schulz, and J. Berakdar, Local and non-local invasive measurements on two quantum spins coupled via nanomechanical oscillations, Symmetry-Basel **12**, 1078 (2020).
[57] Y. Dong, X.-D. Chen, G.-C. Guo, and F.-W. Sun, Robust scalable architecture for a hybrid spin-mechanical quantum entanglement system, Phys. Rev. B **100**, 214103 (2019).
[58] B.-L. Wang, B. Li, X.-X. Li, F.-L. Li, and P.-B. Li, Generation of multiparticle entangled states of nitrogen-vacancy centers with carbon nanotubes, Quantum Inf. Process. **19**, 1 (2020).